Experiments in Fluids 17 (1994) 141–146 © Springer-Verlag 1994

Buoyancy and thermocapillary flow analysis by the combined use of liquid crystals and PIV

G. Wozniak, K. Wozniak

Abstract Thermocapillary and buoyancy convection is studied experimentally using particle-image-velocimetry with liquid crystal tracers for flow visualization and analysis. This method offers the advantage of measuring the entire flow field (velocity field, temperature distribution etc.) in a selected plane within the fluid simultaneously at a given instant of time in contrast to point by point methods like laser-Doppler-velocimetry (LDV). The paper describes the method and presents quantitative results of both, a thermocapillary and a buoyancy flow experiment. Data of the latter are compared with LDV-results and theoretical predictions, respectively.

1 Introduction

For many industrial processes the knowledge of the behaviour of liquid flows due to temperature gradients in the bulk fluid is of fundamental importance as far as heat and mass transfer are concerned. On earth, temperature gradients cause density variations within the fluid, which lead to flows driven by buoyancy forces. However, in orbit buoyancy effects vanish due to the absence of gravity. In this situation fluid motion can be driven by a free surface. This flow is a consequence of the variation of the surface tension with temperature, and is termed thermocapillary convection. While this effect is widely masked by buoyancy effects on Earth, it can play a dominant role under reduced gravity conditions. Present activity areas are solidification front dynamics and material production processes in space motivated by the expectation that the absence of buoyant convection leads to higher quality products. Also bubbles resulting from solidification, melting and other operations present surfaces which can cause thermocapillary convection. Oertel (1979) investigated buoyancy driven flows in rectangular cavities numerically and by means of interferometry. Kao and Kenning (1972) investigated numerically the flow driven by variations in surface tension round a hemispherical gas or vapor bubble on a heated wall for steady state conditions. Raake et al. (1989) measured quantitatively the temperature field near an air bubble in silicon oil under a heated wall by means of interferometry. They also measured the flow velocities by the tracking of tracer particles. Ozawa et al. (1992) investigated the natural convection in a Hele-Shaw cell using thermosensitive liquid-crystal tracers.

The aim of this study is the demonstration and application of a measuring technique, which is capable to capture the velocity and temperature field of a selected flow plane simultaneously, and to apply it to two typical thermoconvective flow configurations:

i) cellular convection in a rectangular cavity heated from below and cooled from above (unstable stratification),
ii) thermocapillary flow driven by a bubble placed under a heated wall.

2 Flow configurations

Figure 1 shows a schematic of the flow type of experiment i). It is the so-called Bénard convection between two horizontal plates. The container geometry of 10:4:1 causes 10 cylindrical convection rolls. The flow is characterized by the Rayleigh-number Ra representing the relative importance of buoyancy forces when compared to viscous forces. Ra is defined as

$$Ra \equiv \frac{g \cdot \beta \cdot \Delta T \cdot h^3}{\nu \cdot a}. \quad (1)$$

In this definition, β denotes the thermal expansion coefficient of the fluid, g the acceleration due to gravity, ΔT the vertical temperature difference, h the distance between the plates, ν the kinematic viscosity and a the thermal diffusivity.

The fluid properties are characterized by the Prandtl-number

$$Pr \equiv \frac{\nu}{a}. \quad (2)$$

The onset of energy transport by cellular convection in an infinitely extended fluid layer takes place at a critical Rayleigh-number of approximately $Ra_c \approx 1708$. In the experiments we used a test cell geometry with internal dimension of 10:4:1 (length:width:height). After exceeding the critical Rayleigh-number (critical temperature difference) by heating the fluid from below ten convection rolls develop.

Received: 18 October 1993 / Accepted: 16 February 1994

G. Wozniak
Technische Universität Bergakademie Freiberg, Institut für Fluidmechanik und Fluidenergiemaschinen, D-09596 Freiberg, Germany

K. Wozniak
Lehrstuhl für Mechanik, Universität GH Essen, D-45117 Essen, Germany

Correspondence to: G. Wozniak

Presented in part at the 6th International Symposium on Applications of Laser Techniques to Fluid Mechanics, Lisbon, Portugal, July 20–23, 1992

Part of the work was financially supported by the "Ministerium für Wissenschaft und Forschung des Landes NW" which is greatfully acknowledged.

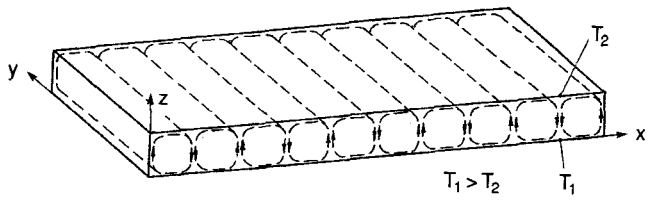

Fig. 1. Bénard convection between two horizontal plates

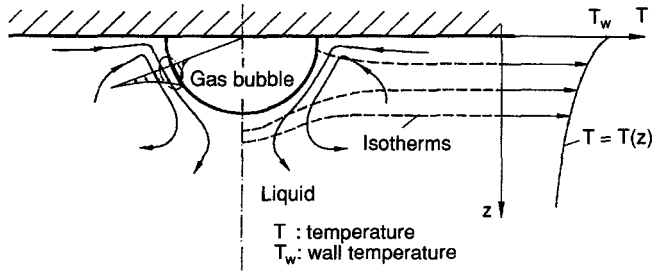

Fig. 2. Mechanism of thermocapillary flow around a bubble under a heated horizontal wall

A schematic of configuration ii) is shown in Fig. 2. A bubble is positioned in a liquid matrix under a heated wall. Temperature variations at a free liquid surface (interface) cause local differences of the interfacial tension which, in turn, induce a flow of liquid near the bubble toward the direction of increasing interfacial tension. Since the surface tension of most liquids decreases with increasing temperature, the flow direction on the periphery of the bubble is from the heated wall towards the bubble pole, where the fluid exhibits lower temperatures. This flow mechanism is characterized by the Marangoni-number defined by

$$Mg \equiv \frac{R^2 \left|\frac{d\sigma}{dT}\right| \left|\frac{dT}{dz}\right|_\infty}{\eta\, a}. \qquad (3)$$

In this definition, R denotes the bubble radius, $|d\sigma/dT|$ the variation of interfacial tension with temperature, $dT/dz|_\infty$ the constant temperature gradient in the bulk fluid far away from the bubble and η the dynamic fluid viscosity. Mg plays the role of a Peclet-number representing the ratio of heat transport by thermocapillary convection to heat transport by pure conduction.

3 Experimental

3.1 Test cells and experiment procedures

3.1.1 Bénard convection

Figure 3 shows a schematic of the test cell of the Bénard experiment (i). It consists of a fluid cell with the inner dimensions of 60 mm × 15 mm × 6 mm (the latter being the fluid layer height). The side wall material is glass for flow visualization

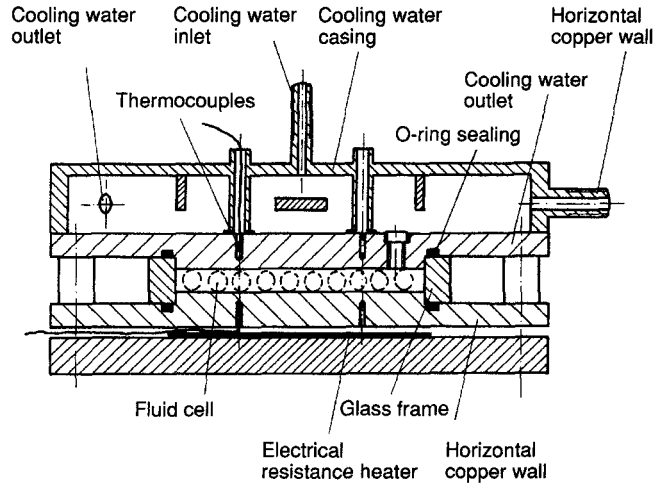

Fig. 3. Test cell of Bénard experiment

purposes and the horizontal end walls consist of copper for uniform plate temperatures. To establish a vertical temperature gradient within the liquid matrix the lower horizontal wall is heated via an electrical resistance heater and the upper wall is cooled by a constant temperature coolant using a common, thermostatically controlled circulator. This loop is linked with the cooling water casing of the chamber via the cooling water inlet and outlet. The glass frame is sealed by two O-rings. Thermocouples located in the horizontal copper plates serve for temperature measurement and control. As test medium water has been used (with liquid crystals as tracer particles in a small concentration, see Sect. 2.2) with a Prandtl-number of $Pr = 7$. The experimental procedure is as follows. First, the upper horizontal wall is heated by the water loop in order to maintain a temperature of $T_1 = 26.5\,^\circ C$. In order to establish a cellular convection at $Ra = 4000$, we calculated a necessary temperature difference of $\Delta T = 1.21$ K following Eq. (1). A Rayleigh-number of $Ra = 4000$ allows to compare with theoretical predictions by Oertel (1979). After 90 minutes quasistationary heating of the lower test cell plate a wall temperature of $T_2 = 27.7\,^\circ C$ was reached and ten cylindrical convection rolls developed. After that, flow visualization and photographic recording have been applied.

3.1.2 Thermocapillary convection

Figure 4 is a schematic of the bubble test cell. It consists of a rectangular cavity with horizontal copper end walls. At each wall a constant, but different, uniform temperature is maintained. To establish a vertical temperature gradient within the liquid matrix, the upper wall is heated via an electrical resistance heater and the lower wall is cooled with a constant temperature coolant by a thermostatically controlled circulator. The inside dimensions of the chamber are 100 mm × 50 mm × 50 mm (width × height × depth). Front and rear side walls consist of optical glass for visualization purposes. In the right side wall a glass window is installed for light sheet illumination. A thermocouple array is positioned vertically near the illuminated midplane for temperature monitoring. In the upper copper wall of the test cell two bore holes with tube

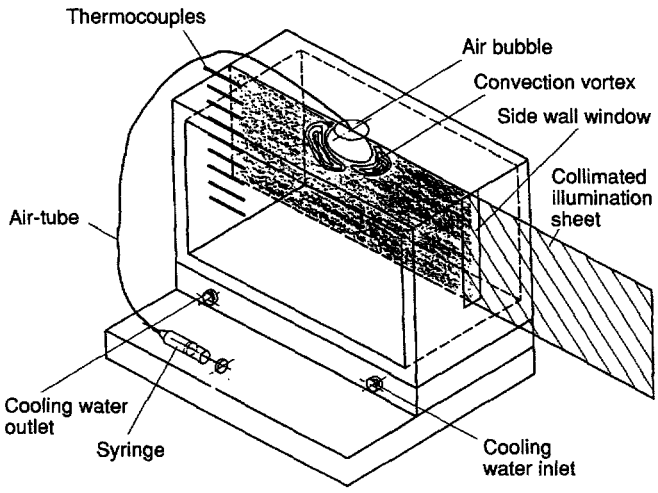

Fig. 4. Schematic of the bubble test chamber

connections are placed in opposite corners. Furthermore, a bore hole for air bubble injection has been installed in the centre of this plate. As test liquid an 87% (by volume) glycerol solution has been used ($Pr = 1220$). The applied temperature gradient in the undisturbed liquid stratification is about 3.6 K/cm.

The experimental procedure is as follows:
First the liquid matrix is heated from above and cooled from below until a steady temperature profile between the horizontal plates within the liquid matrix is established. Then the bubble is injected and the experimenter waits, until a steady convection flow has developed. After that flow visualization and photographic recording can be applied.

3.2
Diagnostic techniques

3.2.1
Particle-image-velocimetry (PIV)

PIV serves to determine the velocity distribution of a flow field quantitatively by means of a multiexposure technique. The aquisition technique for flow fields bases on the record of particle reflections within the flow. With the help of a suitable optical system a thin light sheet is shaped to illuminate a vertical flow plane. The liquid is seeded with tracer particles which scatter the incident light. When the time interval between the exposures is matched to the fluid velocity, the tracers will move a few diameters without loosing their identity. Various local displacements in the illuminated flow field provide characteristic patterns of particle pairs with variable distance and orientation. The velocity field information is stored on photographic material and can be reconstructed by a method explained in the following. The so-called pointwise interrogation technique was employed to evaluate the multiexposed negatives. For that a thin laser beam traverses a multiexposed negative at a certain point of the flow image. Particle images act like point sources, which emit light into the ambient. The superimposed wavelets of each particle image interfere and cause parallel equidistant interference fringes visualized on a screen. The fringes are perpendicular to the direction of the particle displacement. Measuring the fringe spacing and the fringe orientation leads to the local velocity vector of the flow. The resulting interference patterns are evaluated using digital image processing techniques described by Rösgen et al. (1990) and Wozniak et al. (1990).

3.2.2
Liquid crystals and their application to PIV

Our diagnostic method consists of PIV (velocity field) using liquid crystals as tracer particles in order to detect the temperature field of the thermoconvective flows. This way of flow visualization offers the feature of recording velocity field and temperature field data simultaneously. In the described experiments we used encapsulated liquid crystal tracers of about 12 μm in diameter (type TCC 1001, BHD Chemical Ltd.). The concentration of liquid crystals within the test liquids is about 0.1, weight percent. When illuminated with white light this type of liquid crystal reflects light with a wavelength according to the calibration curve shown in Fig. 5.

The first step is to produce a double- or multiexposed colour image of the illuminated flow plane containing the particle tracks and the colour distribution of the thermo chromics. The colour distribution reveals the location of the isotherms. The next step is to transform the chromatic image (negative) onto monochromatic film material. This transformation causes a strong raise of the contrast between the particle images and the background (Guezennec and Kiritsis (1990)). The transformed film material may now be used to reconstruct the velocity field. By application of this procedure the velocity and temperature distribution of thermo-convective liquid flows are simultaneously available.

3.2.3
Optical properties of liquid crystals

The selective reflection in the visible range takes place due to the specific optical properties of the cholesteric liquid crystal substance. Whereas ideal liquids are optically isotropic, liquid crystals exhibit optical characteristics similar to birefringent crystals which are optically anisotropic. The optical properties

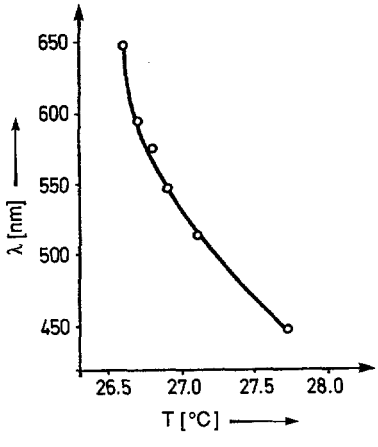

Fig. 5. Reflected wavelength of the liquid crystal TCC 1001 versus temperature

depend on the orientation within the crystal structure (Fig. 6). This special feature of cholesteric liquid crystals is the consequence of many oriented regions that are optically anisotropic. The colour change is directly related to the twist of the structure resulting in a change of orientation of the molecules within the single layers. When changing the temperature, the helical twist of the molecular configuration alters from sheet to sheet. This temperature dependence of the liquid crystal properties is inherent and reversible. The response time of the colour change is of the order of milli-seconds. Only

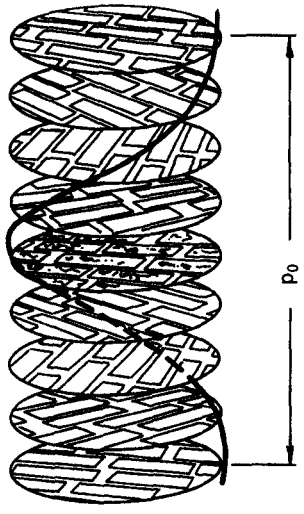

Fig. 6. Structure of cholesteric liquid crystals

incident light possessing the wavelength equal to the helical length p_0 will suffer a reflection. In this case, the path difference between incident beams reflected from adjacent planes is equal to an integral number of wavelength. The beams are in phase and will augment each other to give a reflection maximum into discrete directions. When they are not in phase destructive interference occurs exhibiting a reflection minimum. In general, the colourplay of the liquid crystals is sensitive to a change in the viewing angle. In order to avoid uncertainties due to variations of the viewing angle, the flow phenomena has been recorded at a fixed geometry (orthogonal to the plane of illumination). Detailed information concerning the calibration can be found in Szymczyk et al. (1989).

4
Results and Discussion

4.1
Configuration (i)

Ten convection rolls developed at a selected cavity aspect ratio of 10:4:1. Figure 7 displays the Bénard-convection visualized by the liquid crystal tracer technique, where the four left rolls are magnified. The wavy outline of the thermo-chromatics indicate the location of the isotherms. The velocity distribution was evaluated by means of PIV. Four isotherms resulting from the colour play of the liquid crystals are superposed on the velocity distribution. The colours blue (447 nm), green (514 nm), yellow (585 nm) and red (648 nm) indicate four isotherms. A further colour evaluation would require digital image processing

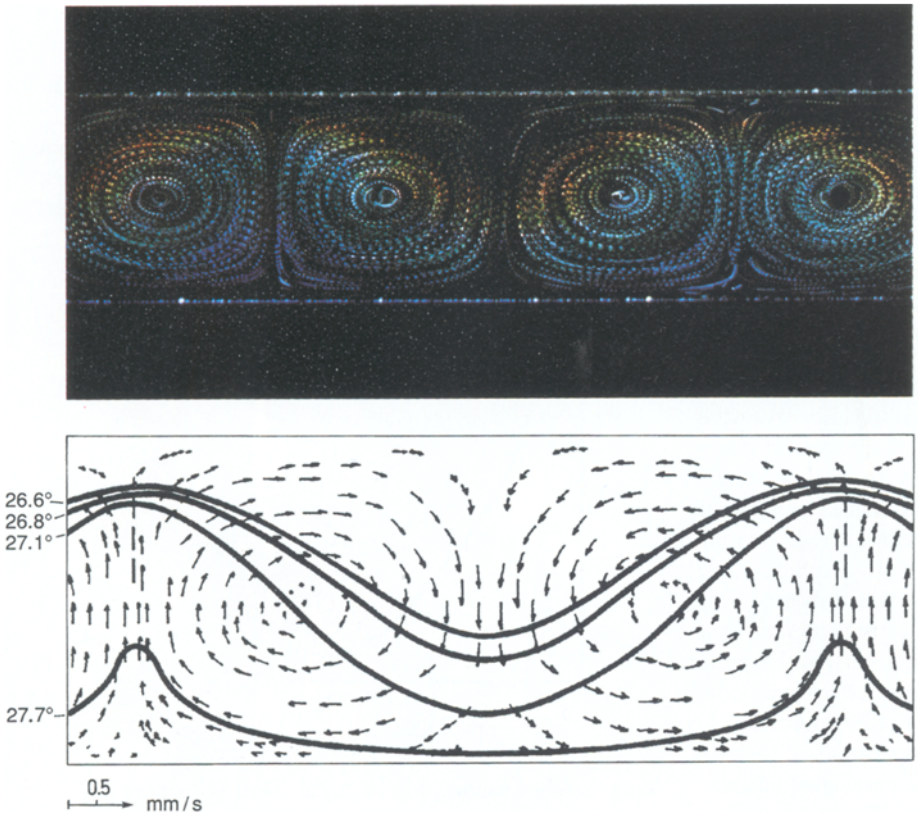

Fig. 7. Colour image and evaluation of convection rolls at $Ra = 4000$

techniques, which can determine two-dimensional temperature distributions automatically; Dabiri and Gharib (1991).

Figure 8 displays scaled vertical velocities of the horizontal midplane obtained by theoretical predictions of Oertel (1979). The superposed LDV and PIV data reveal a satisfying agreement with these numerical results. In the course of our investigations we also used a laser-Doppler-velocimetre (LDV) featuring an integrated Bragg cell. The uncertainty of our measurement is less than 5%. The experimentally obtained vertical velocity data show stronger deviations from theoretical results near the vertical side walls. One reason is the ambient temperature during the experiment, which is 6 Kelvin lower than the upper plate temperature of the test cell and causes a steady thermal loss. This is not taken into account in the theoretical predictions and explains higher velocities of the outer convection rolls. The investigation shows that fluid at the left and right container walls move downwards. Cold fluid on the upper wall sinks due to the higher density. The thermal loss of the side walls causes an additional rise of density and thus of the driving force.

This argument is supported by experimental findings of Oertel (1979). He also found experimentally, that the outer convection rolls circulate faster than his theory predicts. A major reason for the velocity deviations are the simplified and idealized

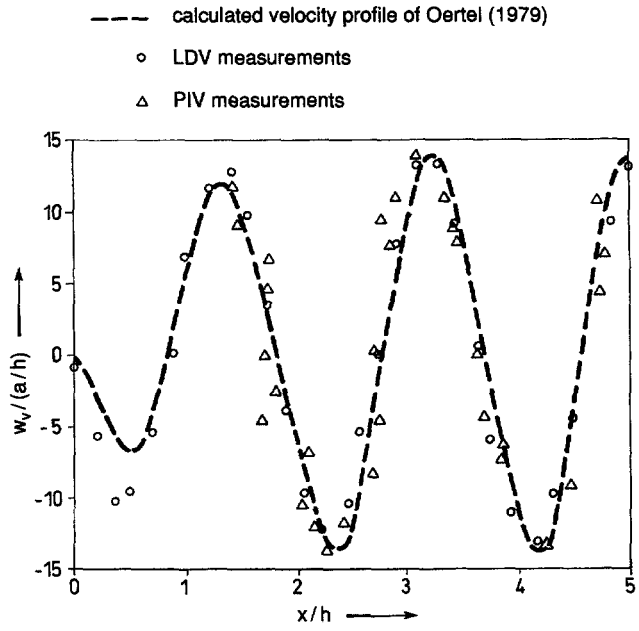

Fig. 8. PIV results and comparison with reference data

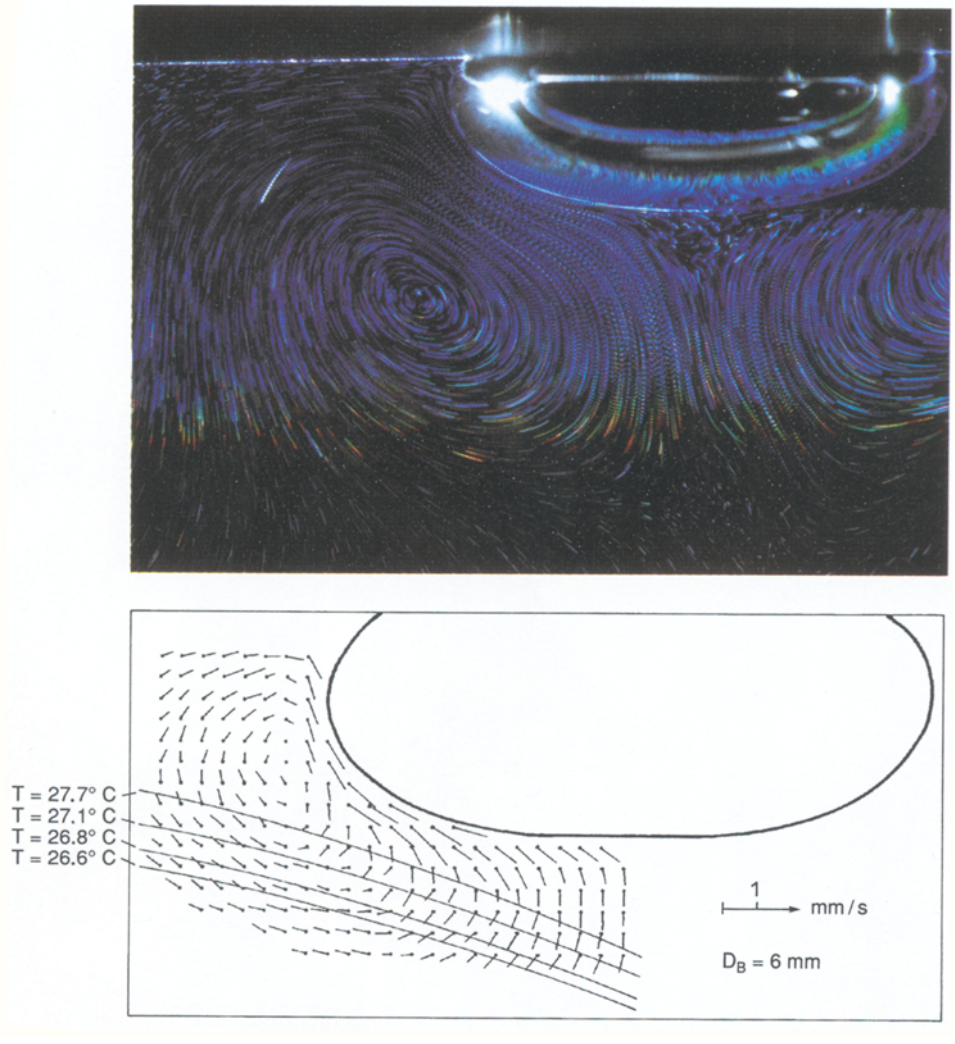

Fig. 9. Colour image of the thermocapillary flow around a bubble and evaluated velocity vectors and isotherms at $Mg = 124$. The horizontal bubble dimension is 1 cm

boundary conditions of Oertels theoretical model. The assumption that the material data are temperature independent causes some additional uncertainties.

4.2
Configuration (ii)

Figure 9 shows a multiple exposed colour image of the thermocapillary flow and the evaluated velocity vectors and isotherms. The bubble was immersed into an 87% (by volume) glycerol solution. The applied temperature gradient in the undisturbed liquid stratification is about 3,6 K/cm. The solution is seeded with encapsulated liquid crystal tracers of about 12 μm in diameter (type TCC 1001, BHD Chemicals Ltd.).

The picture shows two symmetrically arranged vortices within the illuminated plane which are driven by buoyancy and thermocapillary, respectively. The relatively large particle displacements near the bubble contour distinctly demonstrate, that the bubble surface is the principle driver of the flow. The shape of the flow is in qualitative agreement with results of Raake et al. (1989) and Kao and Kenning (1972).

5
Concluding remarks

A novel visualization technique has been applied, which allows to capture temperature- and velocity data of thermo-convective liquid flows simultaneously on a single chromatic image. Besides a quantitative velocity field determination we obtained four isotherms of the flow. Due to the simple and rapid experimental performance we may recommend this technique of flow visualization for buoyancy and thermocapillary liquid convection. The application of liquid crystals for liquid flow visualization is somewhat limited by the fact that suspended crystals and the matrix liquid have to have similar refractive indices.

References

Dabiri D; Gharib M (1991) Digital particle image thermometry: The method and implementation. Exp Fluids 11: 77–86

Guezennec YG; Kiritsis N (1990) Statistical investigation of errors in particle image velocimetry. Exp Fluids 10: 138–146

Kao YS; Kenning DBR (1972) Thermocapillary flow near a hemispherical bubble on a heated wall. J Fluid Mech 53: 715–735

Oertel H Jr; Kirchartz KR (1978) Laser-anemointerferometer for simultaneous measurements of velocity and density. Appl Opt 17, 22: 3535–3538

Ozawa M; Müller U; Kimura T; Takamori T (1992) Flow and temperature measurement of natural convection in a Hele-Shaw cell using a thermosensitive liquid-crystal tracer. Exp Fluids 12: 213–222

Raake D; Siekmann J; Chun Ch-H (1989) Temperature and velocity fields due to surface tension driven flow. Exp Fluids 7: 164–172

Rösgen T; Wozniak K; Wozniak G (1990) Image processing for laser speckle velocimetry using the 2D-fast Fourier transform. Appl Opt 29, 35: 5228–5302

Szymczyk JA; Siekmann J; Chun Ch-H; Wozniak, K (1989) Liquid crystal tracers as a method for thermocapillary flow diagnostics. Arch Mech 41 2–3, 351–360

Wozniak K; Wozniak G; Rösgen T (1990) Particle image velocimetry applied to thermocapillary convection. Exp Fluids 10: 12–16